JOURNAL OF CATALYSIS 133, 358–369 (1992)

Kinetics of Ammonia Decomposition on Vanadium Nitride

S. TED OYAMA

Departments of Chemical Engineering and Chemistry, Clarkson University, Potsdam, New York 13699-5705

Received October 1, 1990; revised August 5, 1991

At high temperatures, above 750 K, the kinetics of ammonia decomposition on vanadium nitride can be described by two irreversible steps, the adsorption of ammonia and the desorption of dinitrogen. There is no partial pressure dependence on nitrogen or hydrogen. This is the same mechanism as that first found on tungsten and will be called the Tamaru mechanism, after its discoverer. First-order and second-order kinetic models fit the data equally well. However, calculation of the preexponential factors give better agreement for the second-order model. Rate parameters for VN are in between those found for Pt and Fe, providing another example where the catalytic properties of an early transition metal carbide or nitride resemble those of a Group VIII metal.

INTRODUCTION

The heterogeneous catalytic synthesis and decomposition of ammonia are important reactions that have been studied widely (*1*). The synthesis reaction allows the fixation of nitrogen and provides the world with an essential feedstock for the production of fertilizers and nitric acid derivatives (*2, 3*). Both the synthesis and decomposition reactions have played important roles in the development of a large number of thermodynamic and kinetic principles (*4*). These topics are covered in a number of reviews (*5, 6*).

This paper deals with a study of the kinetics and mechanism of the ammonia decomposition reaction on vanadium nitride (VN). It was found that the kinetics were similar to those obtained for tungsten (*7*), molybdenum (*8*), iron (*9*), and platinum at high temperature (*10*). The rate was independent of nitrogen and hydrogen partial pressures and was first order in ammonia partial pressure at low temperatures and zero order at high temperatures. Thus, the kinetics agreed with the mechanism first suggested to occur on tungsten (*7*) involving two kinetically significant irreversible (one-way) steps (*11*), the adsorption of ammonia and the desorption of dinitrogen (*6*). This mechanism is henceforth referred to as the Tamaru mechanism, after its discoverer.

$$NH_3 + * \rightarrow \text{immaterial}$$

$$*N_2 \rightarrow N_2 + *$$

In the scheme above * represents empty catalytic sites and/or indicates adsorbed chemical species. Both steps are involved in determining the rate, and there is no single rate-determining process. The kinetics differ from that reported earlier for vanadium nitride at a lower temperature (*12*), in which the Temkin–Pyzhev mechanism was observed.

$$NH_3 + * \rightleftharpoons N^* + \tfrac{3}{2}H_2$$

$$*N_2 \longrightarrow N_2 + *.$$

In this latter mechanism ammonia adsorption is equilibrated and the second step, nitrogen desorption, is rate-determining (*13*). We attribute the difference in the observed kinetics on VN to a transition from the Temkin–Pyzhev mechanism to the Tamaru mechanism with increasing temperature, as predicted theoretically (*6*).

Transition metal carbides and nitrides have been attracting attention because of their high catalytic activity and their resemblance to the Group VIII metals (*14–16*). A

0021-9517/92 $3.00

good correspondence is obtained between the kinetic parameters obtained in this study for VN and those reported for Fe and Pt. This provides another example where the catalytic properties of an early transition metal compound resemble those of a pure metal further to the right in the periodic table (*17*).

EXPERIMENTAL

Catalyst preparation and reaction rate measurements were carried out in a flow system using a tubular 12-mm-o.d. quartz microreactor equipped with a thermowell for temperature monitoring. Typically, 500 mg of V_2O_5 (Puratronic, 99.999%) were employed. Vanadium nitride in the form of a powder was prepared by the temperature-programmed reaction of V_2O_5 in a stream of pure flowing NH_3 (Matheson anhydrous 99.99%). A heating rate of 0.033 K s^{-1}, a final temperature of 1270 K, and a flow rate of 750 μmol s^{-1} (500 cm^3 (NTP)) min^{-1} were used.

For reactivity measurements the VN was used *in situ* without removal from the flow system. Reaction products were monitored by gas chromatography. All rates were measured at atmospheric pressure with the same inlet space velocity based on bed volume of 62400 h^{-1}. Rates are defined as moles of NH_3 decomposed per square centimeter of catalyst per second. Partial pressure variations were carried out by blending He (Matheson, 99.999%) with the NH_3 while keeping the total inlet flow constant. Effects of hydrogen and nitrogen were determined by blending H_2 (Matheson, 99.999%) or N_2 (Matheson, 99.999%) and NH_3, while also maintaining total flows constant. Gases were used as received, except for NH_3, which was passed through a KOH trap to remove water. All lines were thoroughly purged.

For characterization the samples were isolated and transferred to a volumetric adsorption unit for measurement of CO isotherms and BET surface areas. Each sample was evacuated to 10^{-7} Pa at 600 K prior to measurement of a first isotherm at room temperature. Then, the sample was evacuated again to 10^{-7} Pa at room temperature and a second isotherm was taken. The CO uptake was taken to be the difference between the intercepts of the linear portions of the isotherms extrapolated to zero pressure. Subsequent to the CO chemisorption measurements, BET surface area determinations were carried out with the same apparatus. Finally, X-ray diffraction patterns of the samples were obtained.

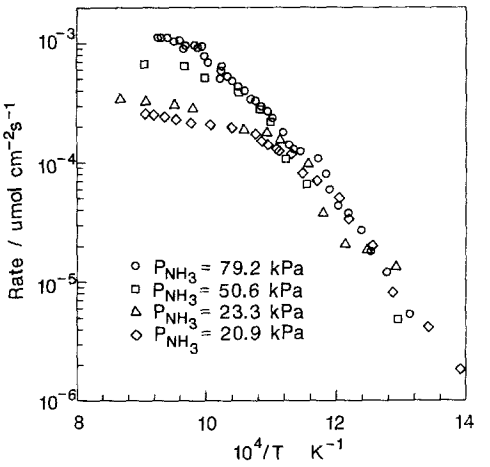

FIG. 1. Arrhenius plot of the rate of ammonia decomposition at atmospheric pressure. Inlet ammonia partial pressure: (○) 79.2 kPa, (□) 50.6 kPa, (△) 23.3 kPa, (◇) 20.9 kPa.

RESULTS

Reactivity measurements were carried out with varying partial pressures of ammonia at different temperatures (Fig. 1). The reaction rates fall in two regions. At low temperatures the rate data for various partial pressures fall on the same line (Fig. 2). At high temperatures the rates flatten out in proportion to the ammonia pressure. Thus, at low temperatures the rate is zero order in ammonia partial pressure, while at high temperatures the rate approaches $P^1_{NH_3}$ (Fig. 3).

Partial pressure variation experiments were carried out with the NH_3 partial pres-

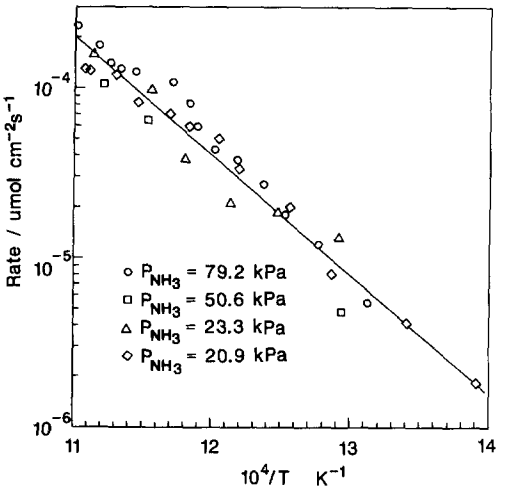

FIG. 2. Rate of ammonia decomposition at low temperatures.

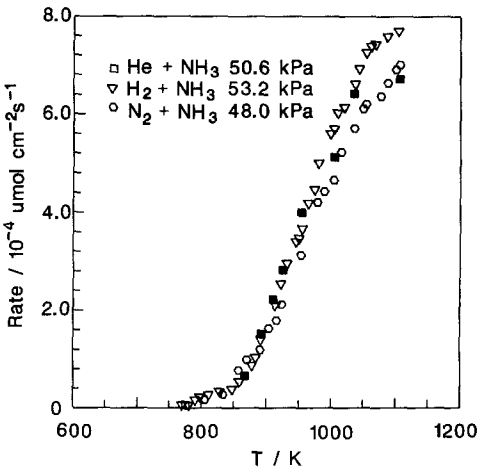

FIG. 4. Hydrogen and nitrogen partial pressure effects in amonia decomposition. Total pressure: 101 kPa. Diluent: (■) He, (▽) H_2, (○) N_2.

sure held close to 50 kPa. This value lies in the middle of the range of ammonia pressures investigated. The rate of NH_3 decomposition at various temperatures hardly changes with the substitution of H_2 and N_2 for He (Fig. 4). The small deviations are due to small variations in the pressure of NH_3.

Measurement of the amount of hydrogen adsorbed at reaction conditions was attempted by monitoring hydrogen in a fast temperature-programmed desorption (TPD) experiment starting from steady-state conditions. The amount of hydrogen evolved was very small compared to that produced

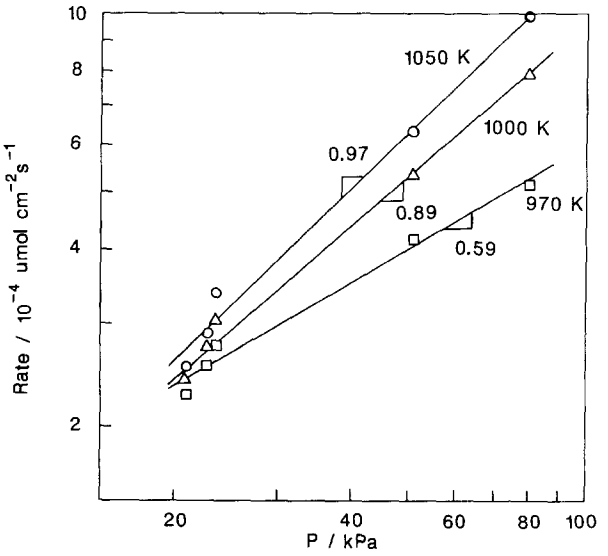

FIG. 3. Ammonia reaction order as a function of temperature. Reaction temperature: (○) 1050 K, (△) 1000 K, (□) 970 K.

by the reaction, measured independently in a slow temperature ramp. This indicated that there was very little adsorbed hydrogen on the surface at reaction conditions.

The BET specific surface area of the sample used in the reactivity measurements was 25.2 $m^2 g^{-1}$ and its CO uptake was 28.8 μmol g^{-1}. The calculated number density of sites was thus 6.9×10^{17} m^{-2}. The X-ray diffraction pattern of the samples matched that of a VN standard of cubic NaCl structure (*18*). Elemental analysis of one of the samples indicated a nitrogen content of 20.1 mol%.

DISCUSSION

Catalyst

The catalyst is identified as VN of the normal cubic structure by X-ray diffraction. No other phases, such as V_3N, V_2N, or V, were detected. Elemental analysis gave 20.1 mol% N, in good agreement with the 21.4 mol% theoretical value expected for VN. The small discrepancy may be due to oxygen remaining in the bulk, a common occurrence in this class of interstitial alloy (*19*). Details of the preparation method are presented elsewhere (*20*). The number density of sites as titrated by CO, 6.9×10^{17} m^{-2}, appears to be substantially below that of a monolayer, $\sim 1 \times 10^{19}$ m^{-2}. This may be due to occupancy of adsorption sites by surface nitrogen atoms, or possibly, contamination of the surface by traces of oxygen. Blockage of sites by nitrogen is more likely because any surface oxygen is probably removed by the high temperature treatment (1270 K) during synthesis.

Reaction Mechanism

The rate of ammonia decomposition does not depend on the partial pressures of nitrogen or hydrogen (Fig. 4). It is also found that hydrogen is not chemisorbed on VN at the conditions of reaction. This behavior is identical to that found on tungsten (*7*) and molybdenum (*8*) and suggests a simple two-step sequence, consisting of two irreversible steps, the adsorption of ammonia and the desorption of dinitrogen. The finding that hydrogen is not present on the surface at reaction conditions indicates that upon adsorption the dehydrogenation of ammonia and the desorption of hydrogen is fast. Together with the observation of a lack of an effect of hydrogen partial pressure, this demonstrates that the adsorption of ammonia is largely irreversible. If the adsorption were reversible, hydrogen would retard the overall rate by driving the equilibrium for the formation of adsorbed nitrogen backward.

$$NH_3 + * \rightleftharpoons N^* + \tfrac{3}{2}H_2.$$

Such an inhibition of the rate by hydrogen is not observed. Similarly, assuming that adsorbed nitrogen is the most abundant reactive intermediate, if nitrogen desorption were reversible, gas-phase dinitrogen should retard the rate by slowing down the measured *net* rate of desorption, which again is not observed.

Rate Expressions

The discussion above presented the main features of the mechanism of the decomposition of ammonia on VN. From this, a limited number of rate expressions may be derived. For an uniform surface, the main consideration is whether nitrogen desorption is first or second order, a question that has been discussed extensively in the past (*21–26*). This gives rise to the two expressions below. For a nonuniform surface reaction, order is not important as the rates of adsorption and desorption depend exponentially on coverage (*27*).

First-order mechanism:

$$NH_3 + * \xrightarrow{k_1} *NH_3 \qquad (1)$$

$$*N_2 \xrightarrow{k_2} N_2 + * \qquad (2)$$

Second-order mechanism:

$$NH_3 + 2* \xrightarrow{k_3} *NH_2 + H* \qquad (3)$$

$$2\,*N \xrightarrow{k_4} N_2 + 2* \qquad (4)$$

TABLE 1

List of Parameters, Units, and Numerical Values

Parameter	Units	Values
k_1	$cm^3\ s^{-1}$	1.68×10^{1} [a]
k_2	s^{-1}	7.74×10^{19} [a]
k_3	$cm^3\ s^{-1}$	6.77×10^{3} [a]
k_4	s^{-1}	3.87×10^{19} [a]
$\frac{1}{2}z$	None	2

[a] At 1003 K.

Non-uniform surface mechanism:

$$NH_3 + S_1 \xrightarrow{k_5} \tfrac{3}{2}H_2 + S_2 \qquad (5)$$

$$S_2 \xrightarrow{k_6} N_2 + S_1. \qquad (6)$$

If steps (1), (3), and (5) are equilibrated, the mechanism corresponds to the Temkin–Phyzev mechanism. Rate expressions may be derived from the first- and second-order models above, assuming that adsorbed nitrogen is the most abundant surface species.

First-order expression:

$$v_1 = \frac{[S]k_1[NH_3]}{[1 + (k_1/k_2)[NH_3]]} \qquad (7)$$

Second-order expression:

$$v_2 = \frac{\frac{1}{2}z[S]k_3[NH_3]}{[1 + (k_3/k_4)^{1/2}[NH_3]^{1/2}]^2} \qquad (8)$$

Non-uniform surface expression:

$$v_n = [S](\pi/f)\sqrt{k_5^0 k_6^0}[NH_3]^{1/2}. \qquad (9)$$

In the expressions above v_1, v_2, and v_n represent the rates of NH_3 decomposition in units of μmol $cm^{-2}\ s^{-1}$, and k_1–k_6 are the rate parameters for steps (1)–(6). $[NH_3]$ is the number density of ammonia in cm^{-3}. $[S]$ is a conversion factor with units of μmol cm^{-2}, which includes the surface area of the catalyst ($25.4 \times 10^4\ cm^2\ g^{-1}$) and Avogadro's number (6.02×10^{17} atoms μmol^{-1}). Table 1 lists the various parameters, together with numerical values and units.

For the second-order case the units of the rate constants are the same as for the first-order treatment. The reason for this is that second-order surface processes require *pairs* of adjacent sites. Thus, dissociative adsorption of ammonia requires not just any two sites, but two sites next to each other. The statistics for such a situation have been analyzed and yields (*28*)

$$(**) = \tfrac{1}{2}z(*)^2/(S),$$

where (**) is the concentration of nearest-neighbor pairs, (*) the concentration of single sites, and z the coordination number surrounding each surface site. This is taken here to be 4, since VN has the NaCl cubic structure. Similarly, associative desorption of nitrogen requires pairs of adjacent adsorbed nitrogen atoms and the same factor, $\frac{1}{2}z$, is applied to this case.

At low temperatures it is expected that nitrogen desorption will become difficult, hence k_2 and k_4 will be small. In this regime the rate expressions for the first- and second-order case become $v_1 = [S]k_2$ and $v_2 = \frac{1}{2}z[S]k_4$, respectively. At high temperatures k_2 and k_4 will be large and the rate expressions become $v_1 = [S]k_1[NH_3]$ and $v_2 = \frac{1}{2}z[S]k_3[NH_3]$, respectively. These limiting expressions are consistent with the observed experimental dependency on NH_3 pressure, zero order at low temperature (Fig. 2), and first order at high temperature (Fig. 3). They also do not show dependency on nitrogen or hydrogen partial pressures, again consistent with experimental results (Fig. 4).

Interestingly, the two rate expressions are of the same form as standard Langmuir–Hinshelwood (L-H) expressions. However, it must be stressed that the expressions do not contain adsorption equilibrium constants and differ fundamentally from L-H equations.

A non-uniform surface analysis can also be carried out using steps (5) and (6) above. In the expression (9) above, f is the width of

the non-uniform distribution (*4*). The expression is obtained by using the exponential forms of the rate of adsorption $v_a = k_5[NH_3]e^{-g\theta}$ (*29*) and the rate of desorption $v_d = k_6 e^{h\theta}$ (*30*), where θ is the coverage, and by applying the steady-state approximation. The expression shows a dependency on $[NH_3]^{1/2}$, and it is clear that the expression does not give a good description of the kinetics.

Reaction Kinetics

The stoichiometry of ammonia decomposition ($NH_3 = \frac{1}{2}N_2 + \frac{3}{2}H_2$) dictates a change in the number of moles with reaction and the kinetic expressions must be integrated over the length of the packed bed. Since the flow is in packed beds (Re = 110) and axial dispersion is low (Pe = 77), concentration profiles will be flat and the reactor can be modeled as a plug flow reactor. A convenient integration method (*31*), useful when the surface area of the catalyst is known, yields

$$\frac{1}{F_{in}y_{in}} = \int \frac{dx}{v}, \qquad (10)$$

where F_{in} is the total inlet molar flow, y_{in} is the fraction of NH_3 in the feed, and v is the reaction rate obtained using $[S]$ or $\frac{1}{2}z[S]$ (Eqs. (7) and (8)). The change in the number of moles is described by

$$[NH_3] = [NH_3]^0\left(\frac{1-x}{1+\varepsilon x}\right), \qquad (11)$$

where ε is an expansion factor defined as the fractional change in volume of the system between no conversion and complete conversion of the reactant (*32*). Substituting (11) into (7), (8), and (9), subsequently into (10), and then integrating gives

First-order model:

$$\frac{1}{F_{in}y_{in}} = \frac{x}{k_2} - \frac{1}{k_1[NH_3]^0}[\varepsilon x + (\varepsilon+1)\ln(1-x)] \qquad (12)$$

Second-order model:

$$\frac{1}{F_{in}y_{in}} = \frac{x}{k_4} - \frac{1}{k_3[NH_3]^0}[\varepsilon x + (\varepsilon+1)\ln(1-x)] + \frac{2}{(k_3k_4[NH_3]^0)^{1/2}}\left\{1 - \sqrt{(1+\varepsilon x)(1-x)} - \frac{(\varepsilon+1)}{2\sqrt{\varepsilon}}\left[\sin^{-1}\left(\frac{\varepsilon - 2\varepsilon x - 1}{\varepsilon+1}\right) - \sin^{-1}\left(\frac{\varepsilon-1}{\varepsilon+1}\right)\right]\right\}. \qquad (13)$$

Non-uniform surface model:

$$\frac{1}{F_{in}y_{in}} = (k_5^0k_6^0[NH_3]^0)^{1/2}\left\{\sqrt{(1+\varepsilon x)(1-x)} - 1 + \frac{(\varepsilon+1)}{2\varepsilon^{1/2}}\left[\sin^{-1}\left(\frac{\varepsilon - 2\varepsilon x - 1}{\varepsilon+1}\right) - \sin^{-1}\left(\frac{\varepsilon-1}{\varepsilon+1}\right)\right]\right\}. \qquad (14)$$

The non-uniform surface analysis was not carried any further as the kinetic rate expression already showed considerable deviation from experimental results. Instead attention was focused on the first- and second-order kinetic expressions. Each expression contains two rate parameters, which in turn are composed of a preexponential factor and an activation energy. The equations were fit by dividing the data into low- and high-temperature regions. In the low-temperature region the rate was zero order and integration of the rate expressions simply gave the first terms in Eqs. (12) and (13). These are identical and simply contain the rate parameters for desorption, k_2 and k_4. In fact, the same expressions can be obtained without integration. The data were fit by linear least-squares and the results are shown by the straight line in Fig. 2. With these parameters available, the other two parameters, k_1 and k_3, were determined for the whole data set using a Simplex fitting routine. Linear and non-linear fitting routines did not converge. The results of the analysis are summarized below.

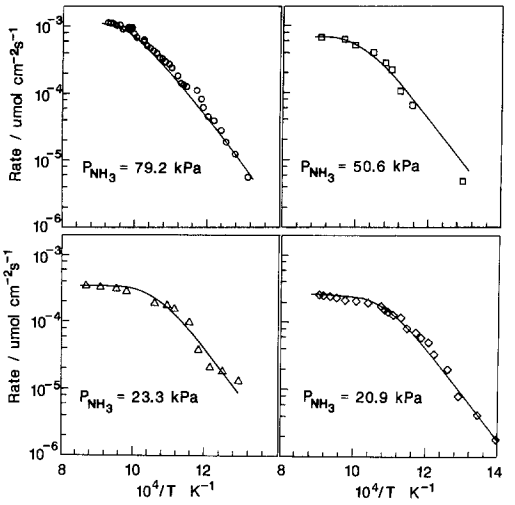

FIG. 5. First-order kinetic models.

First-order fit:

$$k_1 = 2.47 \times 10^3 \exp(-41{,}600/RT) \text{ cm}^3 \text{ s}^{-1} \quad (15)$$

$$k_2 = 8.45 \times 10^{26} \exp(-135{,}000/RT) \text{ s}^{-1}. \quad (16)$$

Second-order fit:

$$k_3 = 9.01 \times 10^3 \exp(-18{,}200/RT) \text{ cm}^3 \text{ s}^{-1} \quad (17)$$

$$k_4 = 4.22 \times 10^{26} \exp(-135{,}000/RT) \text{ s}^{-1}. \quad (18)$$

In the expressions above the activation energy is given in units of J mol^{-1}. As mentioned earlier, the units of the rate constants for the first- and second-order analyses are the same because in the second-order equations the factor $\frac{1}{2}z$ was used in the rate equation (8) to account for the need for adjacent sites in dissociative adsorption and associative desorption. Rate constants k_2 and k_4 were obtained from the same plot (Fig. 2) and differ only by a factor of two, arising from the use of $\frac{1}{2}z$ ($z = 4$).

Both the second-order (Fig. 5) and first-order (Fig. 6) analyses gave calculated curves that closely fit the experimental points (Fig. 1). A χ^2 test (*33*) was performed on each data set to determine the goodness of fit. The fits were very close giving χ^2 values of 0.1351 and 0.1348 for the first-order and second-order analyses, respectively. Thus, the two kinetic models were indistinguishable in their ability to fit the data.

An error analysis on rate parameters k_2 and k_4 was carried out by taking minimum and maximum slopes (Fig. 2). The activation energy was 135,000 ± 11,000 kJ mol^{-1}, and the exponent in the preexponential was 26 ± 1.2. The errors in k_1 and k_3 are more difficult to compute, but similar percentage errors are expected.

Statistical Mechanics Analysis

In order for the parameters of a rate expression to be consistent with their being true rate constants they must satisfy a number of criteria. First, the signs of the activation energy terms must be correct. Second, the magnitudes of the activation energies must conform to expectations for the reactions involved. Finally, the preexponential factors must agree with those calculated

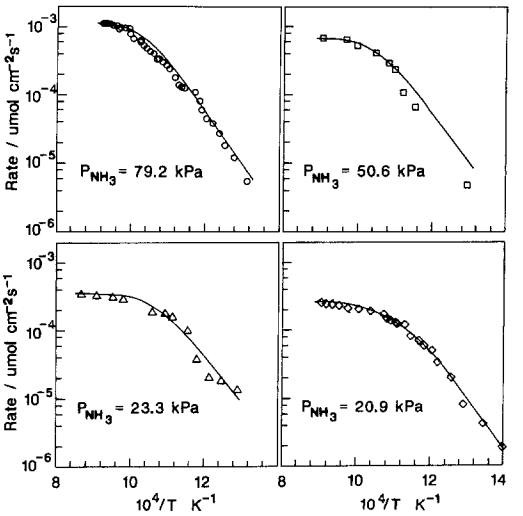

FIG. 6. Second-order kinetic models.

TABLE 2

Comparison of Kinetic Results for Pt, Fe, and VN

Catalyst	NH_3 adsorption		N_2 desorption		$T_{transit}$ (K)
	A ($cm^3\ s^{-1}$)	E ($J\ mol^{-1}$)	A (s^{-1})	E ($J\ mol^{-1}$)	
Pt[a]	9.2×10^2	8,500	2.2×10^{23}	88,000	1107[d]
VN[b]	9.0×10^3	18,200	4.2×10^{26}	135,000	750[e]
Fe[c]	9.8×10^3	42,000	1.6×10^{28}	210,000	<600[e]

[a] Reference (*10*) as reported in (*6*).
[b] This work, second-order fit.
[c] Reference (*9*) as reported in (*6*).
[d] $P_{H_2} = 0.15$ Torr.
[e] Experimental.

with reasonable transition states. Although conformity with these criteria does not prove that the rate parameters are true rate constants, they may be used to rule out a given mechanism. As will be shown, only the second-order mechanism is supported by the calculation of preexponential factors.

The sign and magnitude of the activation energies obtained in this study do fall in the range expected (Table 2) (*5*). As far as the preexponential factors are concerned, a number of criteria exist to test whether the values for equilibrium adsorption constants are physically realistic. These cover associative (*34*) and dissociative (*35*) chemisorption. A recent review surveys preexponential factors for elementary surface processes (*36*). The analysis here follows methods reported in the literature (*37, 38*). The formulas for calculating entropies are reproduced in the appendix (Table 3) together with calculated values at 900 K. Other temperatures gave similar results.

It was found that for both the first-order and second-order cases the adsorption entropy was consistent with the adsorption of ammonia, assuming that the activated complex was immobile and that its rotation was partly hindered (top of Tables 4 and 5). Thus, for the first-order case, adsorption was molecular and the experimental preexponential factor ($2.5 \times 10^3\ cm^3\ s^{-1}$) was in between those calculated for transition states that were immobile and rotating ($9.0 \times 10^4\ cm^3\ s^{-1}$) and immobile and partly rotating ($4.0 \times 10^2\ cm^3\ s^{-1}$). Similarly, for the second-order case, the experimental preexponential factor ($9.0 \times 10^3\ cm^3\ s^{-1}$) was close to that calculated for dissociative adsorption with immobile, but partly rotating, NH_2 groups ($2.2 \times 10^3\ cm^3\ s^{-1}$). Thus, both first- and second-order cases gave reasonable agreement with the measured experimental quantities.

The situation was different for the desorption steps. For the first-order desorption step, making the most favorable assumption of activation from an immobile state to a freely rotating two-dimensional gas did not give good agreement with experiment (bottom of Table 4). The experimental preexponential factor ($8.4 \times 10^{26}\ s^{-1}$) was substantially larger than the calculated value ($8.8 \times 10^{22}\ s^{-1}$). In contrast, the second-order model gave substantially better agreement (bottom of Table 5). The experimental preexponential factor ($4.2 \times 10^{26}\ s^{-1}$) was considerably closer to the calculated value ($1.4 \times 10^{24}\ s^{-1}$). The conclusion from this analysis is that although the kinetic fits of the data agree equally well with both first-order and second order mechanisms, the entropy calculations support only the second-order kinetics. This is satisfactory because dissociation is likely at the high temperatures employed in this study (*5*).

COMPARISONS TO OTHER SYSTEMS

There has been little past work on the vanadium nitride system. A study on metal films reports the formation of VN in the course of the ammonia decomposition reaction (*39*). An investigation comparing different transition metal nitrides reports for VN an activation energy of 125 kJ mol^{-1} in agreement with the low-temperature results obtained here (*40*). The VN sample contained substantial amounts of bulk oxygen, but the surface was likely to be nitrided because of the highly reducing conditions present during reaction. In an extension of this

TABLE 3

Entropy Calculations at 900 K

Type	Degrees of freedom	Species	Formula	Symbol	Value (J/K mol)
Translational	3	N_2	$R \ln[V(2\pi mkT/h^2)^{3/2}] + \frac{3}{2}R$	S_t^3	165
	3	NH_3		S_t^3	159
Translational	2	$*N_2$	$R \ln[A(2\pi mkT/h^2)^1] + R$	S_t^2	110
	2	$*NH_3$		S_t^2	106
	2	$*NH_2$		S_t^2	105
	2	*N		S_t^2	104
	2	*H		S_t^2	82
Rotational	3	NH_3	$R \ln[(\sqrt{\pi}(8\pi^2 IkT)^{3/2}/\sigma h^3] + \frac{3}{2}R$	S_r^3	51
	1	$*NH_3$	$R \ln[(8\pi^2 IkT)^{1/2}/\sigma h] + \frac{1}{2}R$	S_r^3	6
	1	$*NH_2$		S_r^1	20
	1	$*N_2$		S_r^1	22
Vibrational	4	NH_3	$\Sigma R[u/(e^u - 1) - \ln(1 - e^{-u})]$	S_v^4	9
	3	$*NH_2$		S_v^3	3
	1	N≡N		S_v^1	1
	1	N=N		S_v^1	3
	1	N—N		S_v^1	4

Note. $A = V^{2/3}$. $I = \Sigma mr^2$. σ, Symmetry number. $u = h\nu/kT$.

work (*12*) it was found that the kinetics of decomposition of NH_3 in the presence of H_2 followed the Temkin–Pyzhev equation: $v = k[NH_3]/[H_2]^{1.5}$. The kinetics were consistent with equilibrated adsorption of NH_3 and rate-determining desorption of N_2 (*12*). These investigations were carried out in a static system in a lower-temperature regime (690–740 K) than that used in the present studies (750–1100 K). At lower temperatures it is expected that nitrogen desorption will become rate-determining and a change from the tungsten mechanism to the Temkin–Pyzhev mechanism is likely (*6*). Thus, 750 K appears to mark the transition between the two mechanisms.

The values of activation energy obtained in the second-order fits (Eqs. (17)–(18)) fall in between the values for Pt (*10*) and Fe (*9*) as reported in (*6*). These are summarized in Table 2. The values for the preexponential factors also fall in between those of Pt and Fe (Table 2). There is a clear compensation effect with preexponential factors and activation energy values increasing in the same direction.

The transition temperature between the tungsten mechanism and the Temkin–Pyzhev mechanism is given by (*6*):

$$T_{\text{transit}} = \frac{E_d^N - E_d^A}{R \ln[k_{do}^N/(k_{do}^A P_{H_2})]}. \quad (19)$$

In this expression E_d^N and E_d^A are, respectively, the activation energies for desorption of nitrogen and ammonia. The latter step is the reverse of steps (1), (3), or (5) at conditions when the reaction is reversible (Temkin–Phyzev mechanism). Similarly, k_{do}^N and k_{do}^A are the preexponential factors of the rate constants for those steps. In the case of VN the lack of equilibrium adsorption data pre-

TABLE 4

First-Order Analysis

$NH_3 + * \xrightarrow{k_1} *NH_3$

Transition state	Activation entropy	$\Delta S^{\neq}$ (J/K mol)	A_3 ($cm^3\ s^{-1}$)
Mobile, rotating	$S_t^2(*NH_3) - S_t^3(NH_3)$	−53	3.2×10^{10}
Immobile, rotating	$S_t^0(*NH_3) - S_t^3(NH_3)$	−159	9.0×10^4
Immobile, partly rotating	$S_t^0(*NH_3) - S_t^3(NH_3)$ $S_r^1(*NH_3) - S_r^3(NH_3)$	−204	4.0×10^2
—	Experimental fit	−189	2.5×10^3

$*N_2 \xrightarrow{k_2} N_2 + *$

Transition state	Activation entropy	$\Delta S^{\neq}$ ($J\ K^{-1}\ mol^{-1}$)	A_4 (s^{-1})
Mobile molecule	$S_t^3(N_2) - S_t^0(*N_2)$	+165	7.9×10^{21}
Mobile, rotating molecule	$S_t^3(N_2) - S_t^0(*N_2)$ $S_r^1(N_2) - S_r^0(*N_2)$	+168	8.8×10^{22}
—	Experimental fit	+261	8.4×10^{26}

vents the calculation of $T_{transit}$. However, the finding that the experimentally found transition temperature is also in between that of Pt and Fe (Table 2) points to the consistency in the data.

The finding that the parameters for VN are similar to those of Pt and Fe agrees with the general observation that early transition metal carbides and nitrides have catalytic properties similar to those of Group VIII metals (*14, 15*). Metals in the left of the periodic table are electron deficient and react agressively with main group elements (*16*). It has been suggested for WC that alloying with carbon tames the excessive reactivity of tungsten and causes its catalytic behavior to resemble that of platinum (*17*). The resemblance of Mo_2C to Ru and Pd has also been noted (*41*). In the case of Mo it was found for ethane hydrogenolysis that the metal was initially inactive but became activated in the course of reaction because of carburization of the bulk (*42*). Similarly it has been reported that vanadium films are relatively inert in ammonia decomposition but become catalytically active as a result of bulk nitridation (*39*). Thus, it appears that nitridation of early transition metals, like carburization, confers to the element the catalytic properties of metals further to the right in the periodic table.

In summary, the results obtained in this study are consistent with previous kinetic findings on Pt, Fe, and VN. The data may be interpreted globally from the standpoint of the unified mechanism proposed in (*6*). At low temperatures nitrogen desorption is rate-determining, ammonia adsorption is equilibrated, and the reaction follows the Temkin–Phyzev mechanism. At higher temperatures, past a transition point, ammonia adsorption is no longer in equilibrium and the kinetics shift to the Tamaru mechanism.

CONCLUSIONS

The rate of ammonia decomposition on vanadium nitride is zero order in ammonia

TABLE 5

Second-Order Analysis

$NH_3 + 2* \xrightarrow{k_3} *NH_2 + H*$

Transition state	Activation entropy	$\Delta S^{\neq}$ (J/K mol)	A_1 ($cm^3\ s^{-1}$)
Immobile, rotating	$S_t^0(*NH_2) + S_t^0(*H) - S_t^3(NH_3)$	−53	3.2×10^{10}
Immobile, partly rotating	$S_t^0(*NH_2) + S_t^0(*H) - S_t^3(NH_3)$ $S_r^1(*NH_2) - S_r^3(NH_3)$	−190	2.2×10^3
—	Experimental fit	−178	9.0×10^3

$2N* \xrightarrow{k_4} N_2 + 2*$

Transition state	Activation entropy	$\Delta S^{\neq}$ (J/K mol)	A_2 (s^{-1})
Mobile molecule	$S_t^3(N_2) - 2S_t^0(*N)$	+165	7.9×10^{21}
Mobile atoms	$2S_t^3(N) - 2S_t^0(*N)$	+208	1.4×10^{24}
—	Experimental fit	+255	4.2×10^{26}

partial pressure at low temperature and first order at high temperature. The lack of dependence of the rate on nitrogen and hydrogen partial pressures and the lack of adsorbed hydrogen on the surface suggest that the reaction consists of two irreversible steps, the adsorption of ammonia and the desorption of nitrogen. First-order and second-order kinetic models fit the data equally well, but statistical mechanics calculations suggest that only the second-order model gives physically meaningful parameters. These parameters are in agreement with previously reported values for Pt and Fe. The overall findings are consistent with a global view that suggests a shift in kinetics from the Temkin–Phyzev mechanism to the Tamaru mechanism with increasing temperature.

APPENDIX

This Appendix contains details of statistical mechanics calculations employed in the discussion. In these calculations several assumptions that need to be delineated were made. For the translational entropy in three dimensions the volume (V) was obtained from the ideal gas law, $V = RT/N_A P$, and corresponds to a volume per molecule, of magnitude 10^{19} cm^3. However, in two dimensions the area (A) was taken to be $V^{2/3}$, giving a magnitude of 10^{-13} cm^2. In other treatments an arbitrary value of 10^{-15} cm^2 is taken (*36*) or a surface "thickness" 0.6 nm high is assumed (*43*). These differences are not too large for the order-of-magnitude calculations employed here. Importantly, the standard states were taken to be 1 molecule cm^{-3} and 1 molecule cm^{-2} for 3 and 2 degrees of freedom, respectively. These are consistent with the units of concentration used for the gaseous and surface species.

For the vibrational entropy the values of ν employed were 1610, 3210, and 3380 cm^{-1} for adsorbed NH_2; 950, 1630, 3340, and 3410 cm^{-1} for gas-phase NH_3; 2230 cm^{-1} for N≡N; 1600 cm^{-1} for N=N; and 1000 cm^{-1} for N—N (*44*). For the rotational entropy the moments of inertia for NH_3 were calculated from its structure (*45*) and for adsorbed $*NH_2$ assuming that its structure was the same as that in CH_3NH_2 (*45*). All the results are summarized in Table 3.

The rate constants were expressed as $k = A \exp(-E/RT)$, where $A = kT/h \exp(\Delta S^{\neq}/R)$. The units of cm^3 s^{-1} for parameters k_1 and k_3 come from the factor of kT/h and the translational partition function in the entropy expression. The cm^3 corresponds to the loss of 3 translational degrees of freedom for the adsorbing ammonia molecule. The activation entropy, $\Delta S^{\neq}$, was calculated assuming that the activated complex had attributes corresponding to the various species in Table 3. It was found that the greatest contributions were made by the translational and rotational portions of the entropy. The vibrational contributions were small and were not included in this approximate analysis. The results are summarized in Tables 4 and 5.

ACKNOWLEDGMENTS

This work was carried out with support from the Center for Advanced Materials Processing at Clarkson University and the U.S. Department of Energy under the Advanced Coal Research at U.S. Universities Program (Grant no DE-FG22-91 PC91298). The author also acknowledges the assistance of his reactor design class with the Simplex routine analysis and of Rajat Kapoor for the hydrogen TPD experiments.

REFERENCES

1. Bare, S. R., Strongin, D. R., and Somorjai, G. A., *J. Phys. Chem.* **90,** 4726 (1986).
2. Nielsen, A., *Catal. Rev.* **4,** 1 (1970).
3. Nielsen, A., *Catal. Rev. Sci. Eng.* **23,** 17 (1981).
4. Boudart, M., and Djega-Mariadassou, G. "Kinetics of Heterogeneous Catalytic Reactions." Princeton Univ. Press, Princeton, NJ, 1984.
5. Ozaki, A., and Aika, K., *in* "Catalysis Science and Technology" (J. R. Anderson and M. Boudart, Eds.), Vol. 1, p. 87. Springer-Verlag, Berlin, 1981.
6. Tamaru, K., *Acc. Chem. Res.* **21,** 88 (1987).
7. Shindo, H., Egawa, C., Onishi, T., and Tamaru, K., *J. Chem. Soc. Faraday 1* **76,** 280 (1980).
8. Boudart, M., Egawa, C., Oyama, S. T., and Tamaru, K., *J. Chim. Phys.* **78,** 987 (1981).
9. Löffler, D. G., and Schmidt, L. D., *J. Catal.* **44,** 244 (1976).
10. Löffler, D. G., and Schmidt, L. D., *J. Catal.* **41,** 440 (1976).

11. Boudart, M., and Tamaru, K., *Catal. Lett.*, **9**, 15 (1991).
12. McGill, W. J., and Sebba, F., *J. Catal.* **2**, 104 (1963).
13. Temkin, M. I., and Pyzhev, V., *Acta Physicochim. USSR* **12**, 217 (1940).
14. Oyama, S. T., and Haller, G. L., *in* "Catalysis; Specialist Periodical Reports," Vol. 5, pp. 333–365. Roy. Soc. Chem., London, 1982.
15. Leclerq, L., *in* "Surface Properties and Catalysis by Non-Metals" (J. P. Bonnelle, B. Delmon, and E. Derouane, Eds.), p. 433. Reidel, Dordrecht, 1983.
16. Boudart, M., and Oyama, S. T., *in* "Proceedings, 12th Iberoamerican Symp. Catal., Rio de Janeiro," p. 793. Brazilian Petroleum Institute, 1990.
17. Levy, R. B., and Boudart, M., *Science* **181,** 547 (1973).
18. Powder Diffraction File, File number 25-1252, JCPDS International Centre for Diffraction Data, 1980.
19. Toth, L. E., "Transition Metal Carbides and Nitrides." Academic Press, New York, 1971.
20. Kapoor, R., and Oyama, S. T., submitted for publication.
21. Ehrlich, G., *J. Phys. Chem.* **57,** 173 (1955).
22. King, D. A., and Goymour, C. G., *Faraday Trans. 1* **69,** 749 (1973).
23. King, D. A., and Wells, M. G., *Proc. R. Soc. London A* **339,** 245 (1974).
24. Adams, D. L., *Surf. Sci.* **42,** 12 (1974).
25. King, D. A., *Surf. Sci.* **64,** 43 (1977).
26. Gorte, R., and Schmidt, L. D., *Surf. Sci.* **76,** 559 (1978).
27. Brunauer, S., Love, K. S., and Keenan, R. G., *J. Am. Chem. Soc.* **64,** 751 (1942).
28. Boudart, M., *in* "Physical Chemistry, An Advanced Treatise" (H. Eyring, Ed.), Vol. VII. Academic Press, New York, 1975.
29. Zeldowitsch, *Acta Physicochim. USSR* **1,** 449 (1934).
30. Langmuir, I., *J. Am. Chem. Soc.* **54,** 2798 (1932).
31. Iglesia, E., Ph.D. dissertation, Stanford University, 1981.
32. Levenspiel, O., "Chemical Reaction Engineering," 2nd ed., p. 72, Wiley, New York, 1972.
33. Pfaffenberger, R. C., and Patterson, J. H., "Statistical Methods." Richard D. Irwin, Inc., 1987.
34. M. Boudart, D. E. Mears, and M. A. Vannice, *Compte Rendus XXXVI, Ind. Chim. Belge* **32** (special issue), 281 (1967).
35. Vannice, M. A., Hyun, S. H., Kalpakci, B., and Liauh, W. C., *J. Catal.* **56,** 358 (1979).
36. Zhdanov, V. P., Pavlícek, J., and Knor, Z., *Catal. Rev. Sci. Eng.* **30,** 501 (1988).
37. Halford, J. O., *J. Chem. Phys.* **2,** 694 (1934).
38. Glasstone, S., Laidler, K., and Eyring, H., "The Theory of Rate Processes." McGraw–Hill, New York, 1941.
39. Logan, S. R., and Kemball, C., *Trans. Faraday Soc.* **56,** 144 (1960).
40. Lotz, C. R., and Sebba, F., *Trans. Faraday Soc.* **53,** 1246 (1957).
41. Boudart, M., Oyama, S. T., and Leclercq, L., *in* "Proceedings, 7th International Congress on Catalysis, Tokyo, 1980" (T. Seiyama and K. Tanabe, Eds.), p. 578. Kodansha, Tokyo, 1981.
42. Sinfelt, J. H., and Yates, D. J. C., *Nature Phys. Sci.* **229,** 27 (1971).
43. Kemball, C., and Rideal, E. K., *Proc. R. Soc. A* **187,** 73 (1946).
44. Nakamoto, K., "Infrared and Raman Spectra of Inorganic and Coordination Compounds," 3rd ed., Wiley, New York, 1978.
45. Weast, R. C., Ed., "CRC Handbook of Chemistry and Physics," 61st ed. CRC Press, Boca Raton, FL, 1981.